OPEN ACCESS Freely available online

PLOS ONE

Mixed Convection Peristaltic Flow of Third Order Nanofluid with an Induced Magnetic Field

Saima Noreen*

Department of Mathematics, Comsats Institute of Information Technology, Park Road, Chak Shahzad, Islamabad, Pakistan

Abstract

This research is concerned with the peristaltic flow of third order nanofluid in an asymmetric channel. The governing equations of third order nanofluid are modelled in wave frame of reference. Effect of induced magnetic field is considered. Long wavelength and low Reynolds number situation is tackled. Numerical solutions of the governing problem are computed and analyzed. The effects of Brownian motion and thermophoretic diffusion of nano particles are particularly emphasized. Physical quantities such as velocity, pressure rise, temperature, induced magnetic field and concentration distributions are discussed.

Citation: Noreen S (2013) Mixed Convection Peristaltic Flow of Third Order Nanofluid with an Induced Magnetic Field. PLoS ONE 8(11): e78770. doi:10.1371/journal.pone.0078770

Editor: Sefer Bora Lisesivdin, Gazi University, Turkey

Received August 7, 2013; **Accepted** September 17, 2013; **Published** November 18, 2013

Funding: This paper was funded by the Deanship of Scientific Research (DSR), King Abdulaziz University (KAU), under grant no. 25-130/1433 HiCi. The author, therefore, acknowledges technical and financial support of KAU. The support is in the form of project for academic research at KAU. This is to certify that this work is not funded through any external source/research organization including industry etc. The funders had no role in study design, data collection and analysis, decision to publish, or preparation of the manuscript.

Competing Interests: The author has declared that no competing interests exist.

* E-mail: laurel_lichen@yahoo.com

Introduction

Peristaltic motion is now an important research topic due to its immense applications in engineering and physiology. This type of rhythmic contraction is the basis of peristaltic pumps that move fluids through tubes without direct contact with pump components. This is a particular advantage in biological/medical applications where the pumped material need not to contact any surface except the interior of the tube. The word "peristalsis" comes from a Greek word "Peristaltikos"which means clasping and compressing. The peristaltic flow has specific involvement in the transport of urine from kidney to the bladder, chyme movement in gastrointestinal tract, movement of ovum in the female fallopian tubes, blood circulation in the small blood vessels, roller and finger pumps, sanitary fluid transport and many others. Latham [1] and Shapiro et al. [2] reported initial studies for the peristaltic flow of viscous fluid. Since then ample attempts have been made for peristalsis in symmetric flow geometry (seefewrecentstudies [3–8]). Recently, physiologists argued that the intra-uterine fluid flow (because of mymometrical contractions) represents peristaltic mechanism and the myometrical contractions may appear in both asymmetric and symmetric channels [9]. Hence some researchers [10–15] discussed the peristaltic transport in an asymmetric channel with regard to an application of intra-uterine fluid flow in a nonpregnant uterus.

Heat transfer in cooling processes is quite popular area of industrial research. Conventional methods for increasing cooling rates include the extended surfaces such as fins and enhancing flow rates. These conventional methods have their own limitations such as undesirable increase in the thermal management system's size and increasing pumping power respectively. The thermal conductivity characteristics of ordinary heat transfer fluids like oil, water and ethylene glycol mixture are not adequate to meet today's requirements. The thermal conductivity of these fluids have key role in heat transfer coefficient between the heat transfer medium and heat transfer surface. Hence many techniques have been proposed for improvement in thermal conductivity of ordinary fluids by suspending nano particles in liquids. The term "nano" introduced by Choi [16] describes a liquid suspension containing ultra-fine particles (diameter less than 50 nm). The nanoparticle can be made of metal, metal oxides, carbide, nitride and even immiscible nano scale liquid droplets. Although the literature on flow of viscous nanofluid has grown during the last few years (see [17–32] andmanyrefs.therein) but the information regarding peristaltic flow of nano fluids is yet scant. To our information, Akbar and Nadeem [33] studied the peristaltic flow of viscous nanofluid with an endoscope. Influence of partial slip in peristaltic flow of viscous fluid is explained by Akbar et al. [34].

The aim of present study is to venture further in the regime of peristalsis for fluids with nanoparticles. Therefore we examine here the mixed convective peristaltic transport of third order nanofluid in an asymmetric channel. Channel asymmetry is produced by peristaltic waves of different amplitude and phases. Mathematical modelling involves the consideration of induced magnetic field, Brownian motion and thermophorsis effects. Numerical solution of nonlinear problem is obtained using shooting method. Limiting case for viscous nanofluid in symmetric channel is also analyzed. Detailed analysis for the quantities of interest is seen.

Physical Model

Extra stress tensor $\bar{\mathbf{S}}$ for third order fluid model is given by

$$\mathbf{T} = -p\mathbf{I} + \mathbf{S}, \tag{1}$$

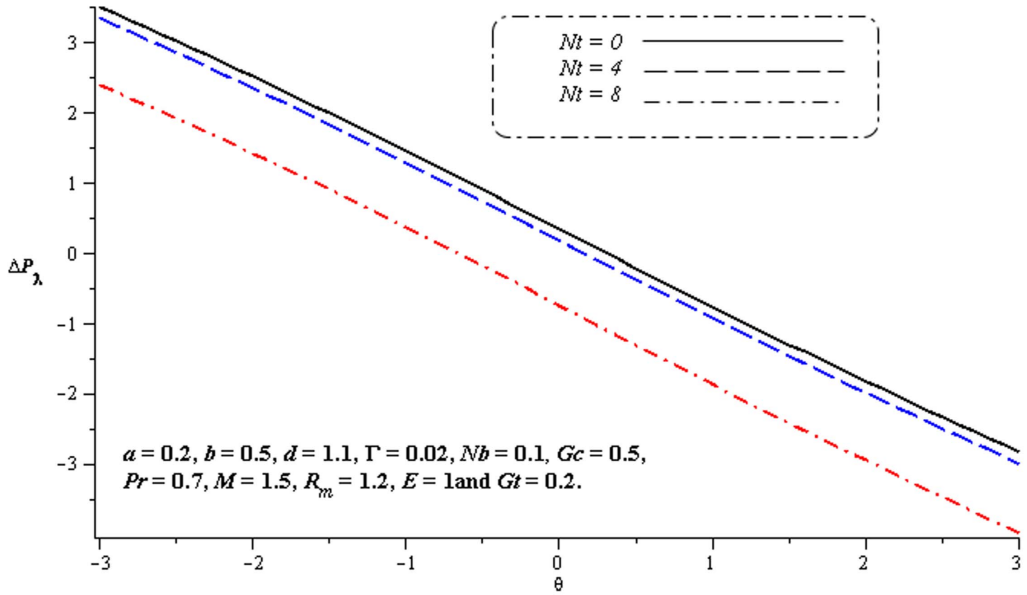

Figure 1. Influence of Nt on ΔP_λ.
doi:10.1371/journal.pone.0078770.g001

$$\mathbf{S}=\mu\mathbf{A_1}+\epsilon_1\mathbf{A_2}+\epsilon_2\mathbf{A_1^2}+\beta_1\mathbf{A_3}+\beta_2(\mathbf{A_2A_1}+\mathbf{A_1A_2})+\beta_3\left(\mathrm{tr}A_1^2\right)A_1, \quad (2)$$

$$\mathbf{A}_1=\mathbf{L}+\mathbf{L}^T,\ \mathbf{A}_2=\frac{d\mathbf{A}_1}{dt}+\mathbf{A}_1\mathbf{L}+\mathbf{L}^T\mathbf{A}_1,\ \mathbf{L}=\mathrm{grad}\mathbf{V}, \quad (3)$$

in which $\mathbf{I}$, p, μ, $\mathbf{S}$ and $\mathbf{A}_1$, $\mathbf{A}_2$ respectively stand for the identity tensor, the pressure, the fluid dynamic viscosity, the extra stress tensor and the first and second Rivlin Ericksin tensors in which the material parameters ϵ_i; $i(i=1-2)$ and β_i; $i(i=1-3)$ must satisfy

$$\mu\geq 0,\ \epsilon_1\geq 0,|\epsilon_1+\epsilon_2|\leq\sqrt{24\mu\beta_3},\beta_1+\beta_2=0,\ \beta_2\geq 0.$$

In the absence of displacement current, the Maxwell's equations are

$$\nabla\cdot\mathbf{E}=0,\quad \nabla\times\mathbf{E}=-\mu_e\frac{\partial\mathbf{H}}{\partial t},\quad \nabla\times\mathbf{H}=\mathbf{J},\quad \nabla\cdot\mathbf{H}=0, \quad (4)$$

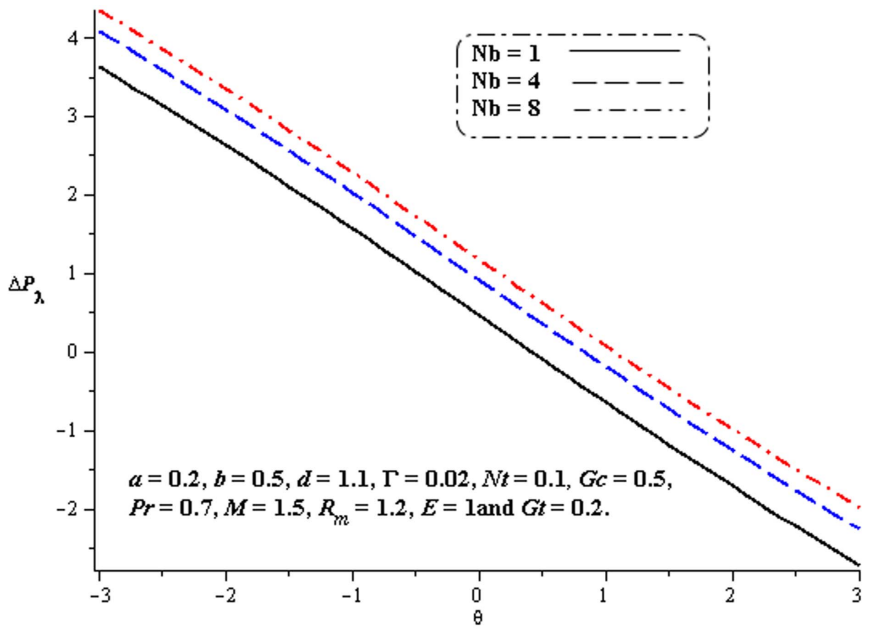

Figure 2. Influence of Nb on ΔP_λ.
doi:10.1371/journal.pone.0078770.g002

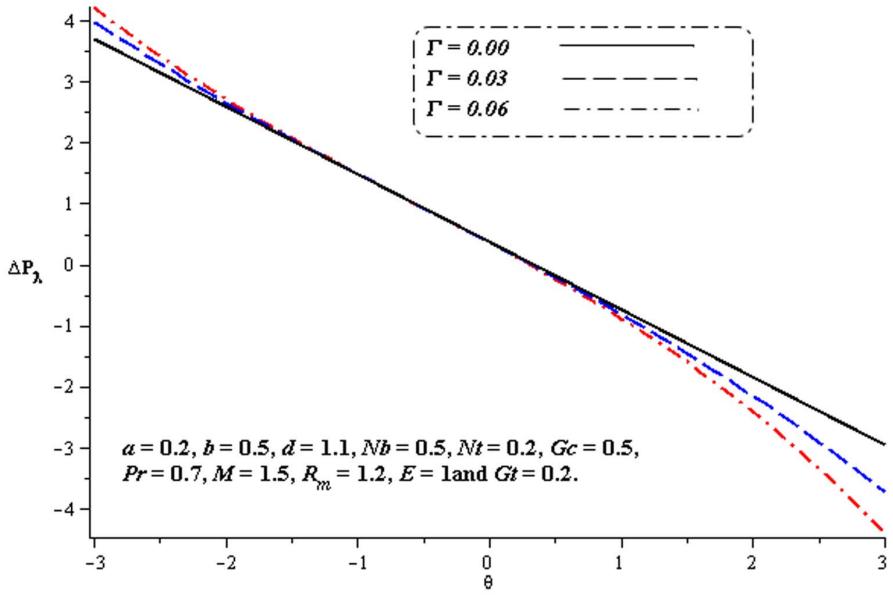

Figure 3. Influence of Γ on ΔP_λ.
doi:10.1371/journal.pone.0078770.g003

$$\mathbf{J}=\sigma(\mathbf{E}+\mu_e(\mathbf{V}\times\mathbf{H})). \tag{5}$$

Mathematical Formulation

Consider third order nanofluid in an asymmetric channel of width d_1+d_2. Let c be the speed by which sinusoidal wavetrains propagate along the channel walls. The $\bar{X}$ and $\bar{Y}$-axes in the rectangular coordinates $(\bar{X},\bar{Y})$ system are taken parallel and transverse to the direction of wave propagation, respectively. A constant magnetic field of strength H_0 acts in the transverse direction resulting in an induced magnetic field $\mathbf{H}(\bar{h}_{\bar{x}}(\bar{X},\bar{Y},\bar{t}),\bar{h}_{\bar{y}}(\bar{X},\bar{Y},\bar{t}),0)$. The total magnetic field is $\mathbf{H}^+(\bar{h}_{\bar{x}}(\bar{X},\bar{Y},\bar{t}),H_0+\bar{h}_{\bar{y}}(\bar{X},\bar{Y},\bar{t}),0)$. Further the lower wall is maintained at temperature T_0 and nano particles concentration C_0 while the temperature and nanoparticles concentration at the upper wall are T_1 and C_1 respectively. The wall surfaces satisfy

$$\bar{h}_1(\bar{X},\bar{t})=\bar{d}_1+\bar{a}_1\cos\left(\frac{2\pi}{\lambda}(\bar{X}-c\bar{t})\right).....\text{upper wall},$$

$$\bar{h}(\bar{X},\bar{t})=\bar{d}_2+\bar{a}_2\cos\left(\frac{2\pi}{\lambda}(\bar{X}-c\bar{t})+\phi'\right).....\text{lower wall}, \tag{6}$$

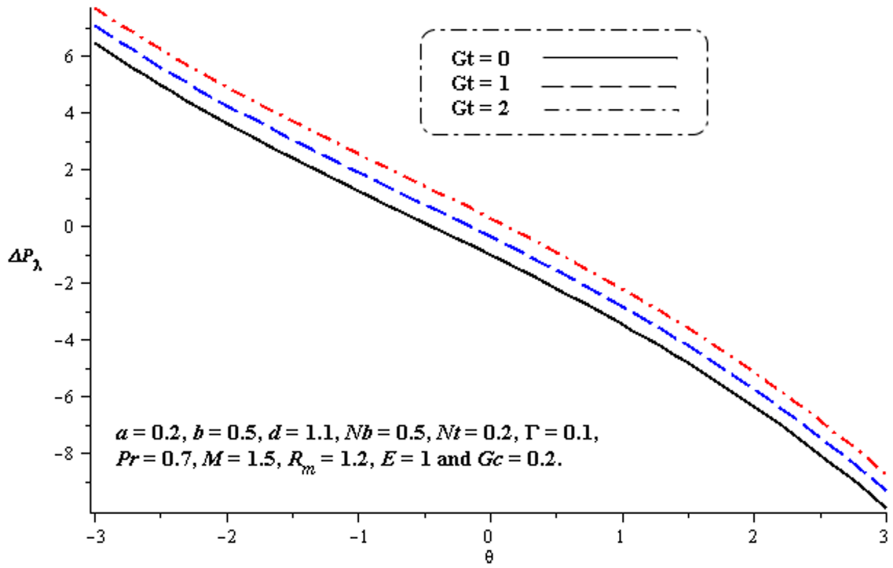

Figure 4. Influence of Gt on ΔP_λ.
doi:10.1371/journal.pone.0078770.g004

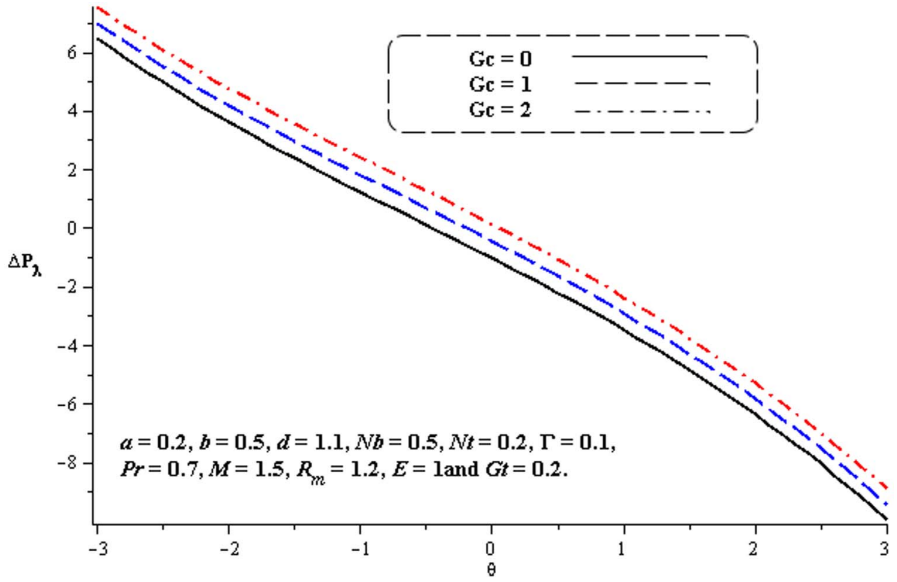

Figure 5. Influence of Gc on ΔP_λ.
doi:10.1371/journal.pone.0078770.g005

where $\bar{a}_1, \bar{a}_2$ are the wave amplitudes and the phase difference ϕ' varies in the range $0 \le \phi' \le \pi$. The case $\phi' = 0$ is subjected to the symmetric channel with waves out of phase and the waves are in phase for $\phi = \pi$. Further λ is the wavelength, $\bar{t}$ the time and $\bar{a}_1, \bar{a}_2, \bar{d}_1, \bar{d}_2$ and ϕ satisfy $\bar{a}_1^2 + \bar{a}_2^2 + 2\,\bar{a}_1\bar{a}_2 \cos\phi' \le (\bar{d}_1 + \bar{d}_2)^2$. Denoting the velocity components $\bar{U}$ and $\bar{V}$ along the $\bar{X}$ and $\bar{Y}-$directions in the fixed frame, one can write $\mathbf{V}$ as

$$\mathbf{V} = [\bar{U}(\bar{X}, \bar{Y}, \bar{t}), \bar{V}(\bar{X}, \bar{Y}, \bar{t}), 0]. \tag{7}$$

The fundamental equations governing the flow of an incompressible fluid are

$$\nabla \cdot \mathbf{V} = 0. \tag{8}$$

$$\rho \frac{d\mathbf{V}}{dt} = \mathrm{div}\mathbf{T} + \mu_e(\nabla \times \mathbf{H}^+) \times \mathbf{H}^+ + \rho \mathbf{g} \ell (\bar{T} - T_0) + \rho g \ell (\bar{C} - C_0), \tag{9}$$

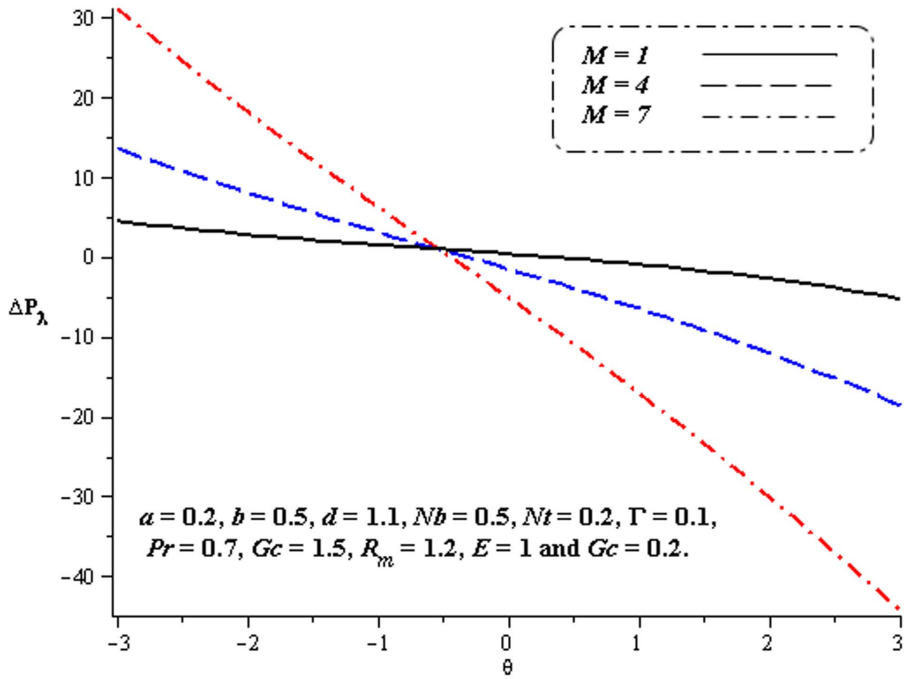

Figure 6. Influence of M on ΔP_λ.
doi:10.1371/journal.pone.0078770.g006

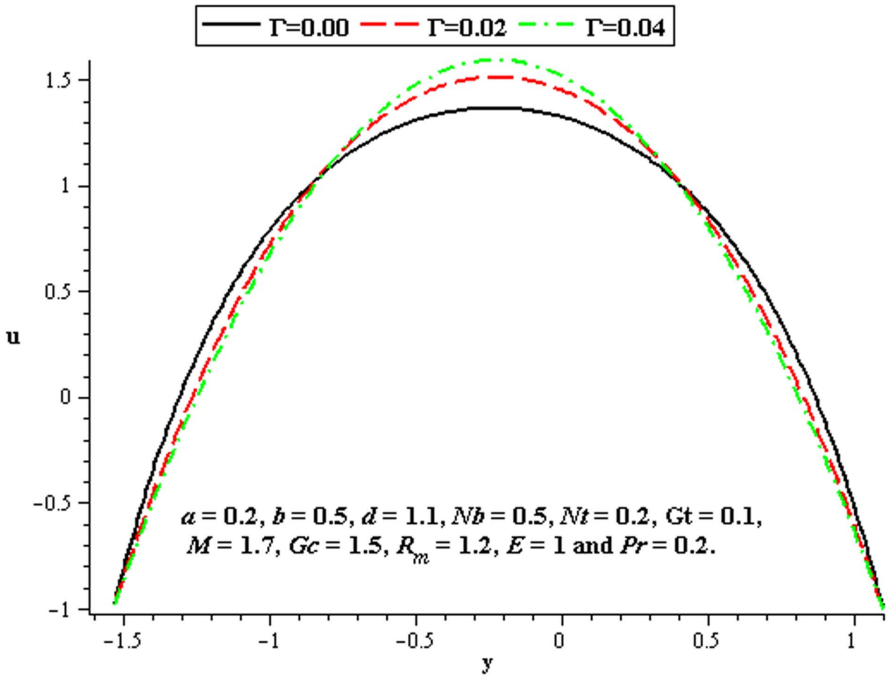

Figure 7. Influence of Γ on *u*.
doi:10.1371/journal.pone.0078770.g007

$$\rho\left[\frac{\partial}{\partial \bar{t}}+\bar{U}\frac{\partial}{\partial \bar{X}}+\bar{V}\frac{\partial}{\partial \bar{Y}}\right]\bar{T}=\kappa\left[\frac{\partial^2 \bar{T}}{\partial X^2}+\frac{\partial^2 \bar{T}}{\partial Y^2}\right]+\tau\left[D_B\left(\frac{\partial \bar{C}}{\partial \bar{x}}\frac{\partial \bar{T}}{\partial \bar{x}}+\frac{\partial \bar{C}}{\partial y}\frac{\partial \bar{T}}{\partial y}\right)+\frac{D_T}{T_m}\left\{\left(\frac{\partial \bar{T}}{\partial \bar{x}}\right)^2+\left(\frac{\partial \bar{T}}{\partial \bar{y}}\right)^2\right\}\right], \tag{10}$$

$$\left[\frac{\partial}{\partial \bar{t}}+\bar{U}\frac{\partial}{\partial \bar{X}}+\bar{V}\frac{\partial}{\partial \bar{Y}}\right]\bar{C}=D_B\left[\frac{\partial^2 \bar{C}}{\partial \bar{X}^2}+\frac{\partial^2 \bar{C}}{\partial \bar{Y}^2}\right]+\frac{D_T}{T_m}\left[\frac{\partial^2 \bar{T}}{\partial \bar{X}^2}+\frac{\partial^2 \bar{T}}{\partial \bar{Y}^2}\right], \tag{11}$$

$$\frac{d\mathbf{H}^+}{dt}=\nabla\times(\mathbf{V}\times\mathbf{H}^+)+\frac{1}{\varsigma}\nabla^2\mathbf{H}^+, \tag{12}$$

in which ρ denotes the density of fluid, D_T the thermophoretic diffusion coefficient, T the temperature, $\bar{C}$ the concentration, ℓ the thermal conductivity, g the acceleration due to gravity, $\bar{p}$ is the pressure, D_B is Brownian diffusion coefficient, $\tau=(\rho c_1)_p/(\rho c_1)_f$ the ratio of the specific heat capacity of the nanoparticle material and heat capacity of the fluid, κ the thermal diffusivity, c_1 is the volumetric volume expansion coefficient, and ρ_p is the density of the particle, $\bar{S}_{\bar{X}X}$, $\bar{S}_{\bar{X}\bar{Y}}$, $\bar{S}_{\bar{Y}\bar{Y}}$ are components of extra stress tensor $\mathbf{S}$ and $\varsigma=\sigma\mu_e$ is the magnetic diffusivity.

To facilitate the analysis, we introduce the following transformations between fixed and wave frames

$$\bar{x}=\bar{X}-c\bar{t},\qquad \bar{y}=\bar{Y},\qquad \bar{p}(\bar{x},\bar{y})=\bar{P}(\bar{X},\bar{Y},\bar{t})$$

$$\bar{u}(\bar{x},\bar{y})=\bar{U}-c,\qquad \bar{v}(\bar{x},\bar{y})=\bar{V}. \tag{13}$$

in which $(\bar{u},\bar{v})$ are the velocity components in the wave frame.

Equations (1)–(12) in terms of above transformations give

$$\frac{\partial \bar{u}}{\partial \bar{x}}+\frac{\partial \bar{v}}{\partial \bar{y}}=0, \tag{14}$$

$$\rho\left(\bar{u}\frac{\partial}{\partial \bar{x}}+\bar{v}\frac{\partial}{\partial \bar{y}}\right)\bar{u}+\frac{\partial \bar{p}_m}{\partial \bar{x}}=\frac{\partial \bar{S}_{xx}}{\partial \bar{x}}+\frac{\partial \bar{S}_{xy}}{\partial \bar{y}}+\rho g\kappa(\bar{T}-T_0)+\rho g\kappa(\bar{C}-C_0)-\frac{\mu_e}{2}\left(\frac{\partial H^{+2}}{\partial \bar{x}}\right)+\mu_e\left(\bar{h}_{\bar{x}}\frac{\partial \bar{h}_x}{\partial \bar{x}}+\bar{h}_{\bar{y}}\frac{\partial \bar{h}_x}{\partial \bar{y}}+H_0\frac{\partial \bar{h}_x}{\partial \bar{y}}\right), \tag{15}$$

$$\rho\left(\bar{u}\frac{\partial}{\partial \bar{x}}+\bar{v}\frac{\partial}{\partial \bar{y}}\right)\bar{v}+\frac{\partial \bar{p}_m}{\partial \bar{y}}=\frac{\partial \bar{S}_{yx}}{\partial \bar{x}}+\frac{\partial \bar{S}_{yy}}{\partial \bar{y}}-\frac{\mu_e}{2}\left(\frac{\partial H^{+2}}{\partial \bar{y}}\right)+\mu_e\left(\bar{h}_{\bar{x}}\frac{\partial \bar{h}_{\bar{y}}}{\partial \bar{x}}+\bar{h}_{\bar{y}}\frac{\partial \bar{h}_{\bar{y}}}{\partial \bar{y}}+H_0\frac{\partial \bar{h}_{\bar{y}}}{\partial \bar{y}}\right), \tag{16}$$

$$\rho\left[\bar{u}\frac{\partial}{\partial \bar{x}}+\bar{v}\frac{\partial}{\partial \bar{y}}\right]\bar{T}=\kappa\left[\frac{\partial^2 \bar{T}}{\partial \bar{x}^2}+\frac{\partial^2 \bar{T}}{\partial \bar{y}^2}\right]+\tau\left[D_B\left(\frac{\partial \bar{C}}{\partial \bar{x}}\frac{\partial \bar{T}}{\partial \bar{x}}+\frac{\partial \bar{C}}{\partial y}\frac{\partial \bar{T}}{\partial y}\right)+\frac{D_T}{T_m}\left\{\left(\frac{\partial \bar{T}}{\partial \bar{x}}\right)^2+\left(\frac{\partial \bar{T}}{\partial \bar{y}}\right)^2\right\}\right], \tag{17}$$

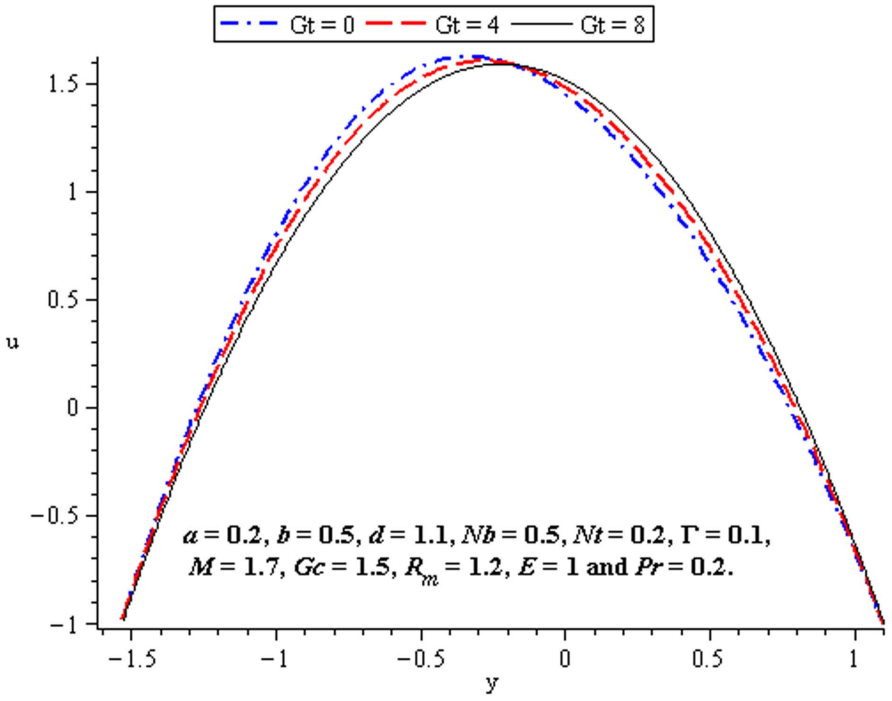

Figure 8. Influence of *Gt* on *u*.
doi:10.1371/journal.pone.0078770.g008

$$\left[\bar{u}\frac{\partial}{\partial\bar{x}}+\bar{v}\frac{\partial}{\partial\bar{y}}\right]\bar{C}=D_B\left[\frac{\partial^2\bar{C}}{\partial\bar{x}^2}+\frac{\partial^2\bar{C}}{\partial\bar{y}^2}\right]+\frac{D_T}{T_m}\left[\frac{\partial^2\bar{T}}{\partial\bar{x}^2}+\frac{\partial^2\bar{T}}{\partial\bar{y}^2}\right], \quad (18)$$

$$\frac{\partial\bar{E}}{\partial y}=\frac{\partial}{\partial y}\left(\bar{u}+\bar{u}\bar{h}_y-\bar{v}\bar{h}_x\right)+\frac{1}{R_m}\left(\delta^2\frac{\partial^2}{\partial x^2}+\frac{\partial^2}{\partial y^2}\right)\bar{h}_x, \quad (19)$$

Defining $Gc, Pr, Gt, Nb, Nt, R_m, M$ as mass Grashof number, Prandtl number, local temperature Grashof number, Brownian

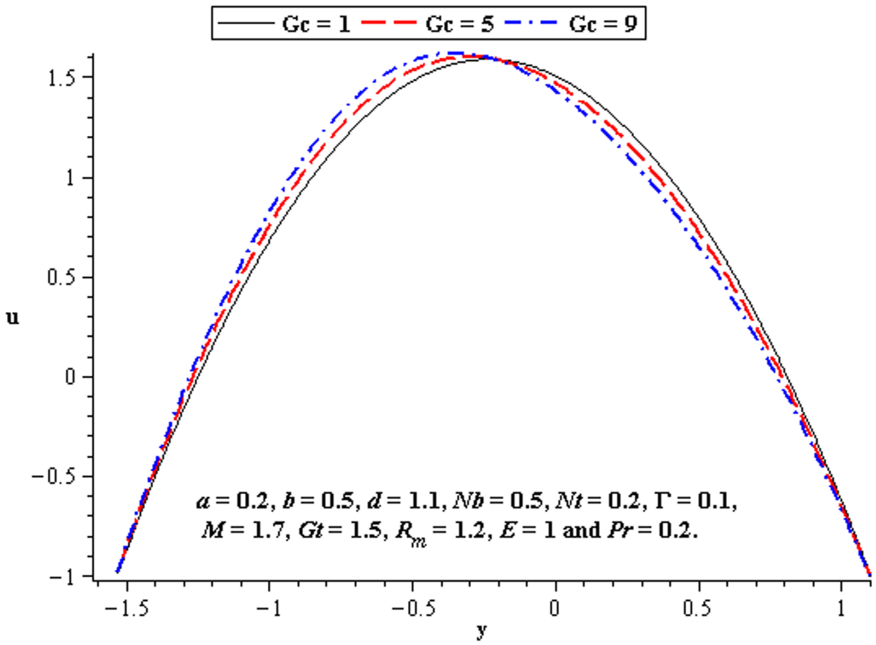

Figure 9. Influence of *Gc* on *u*.
doi:10.1371/journal.pone.0078770.g009

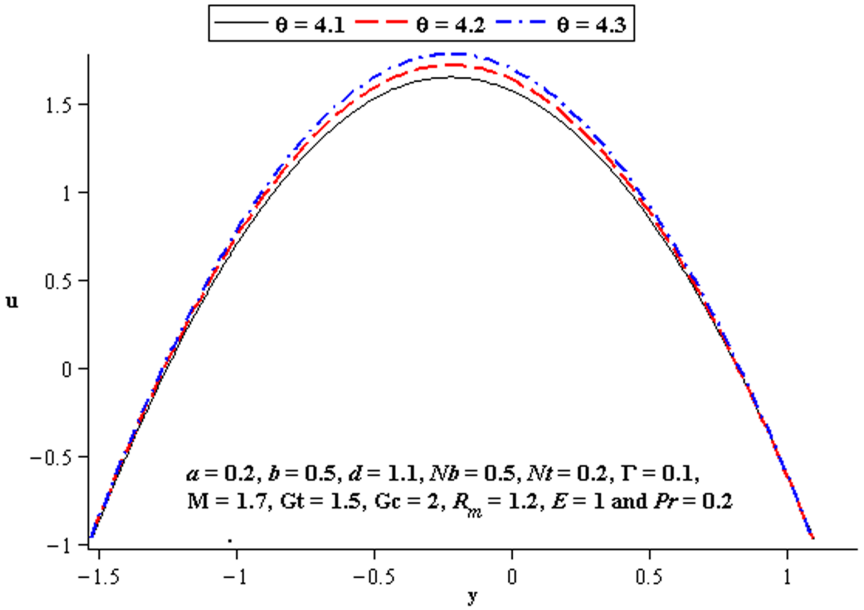

Figure 10. Influence of θ on u.
doi:10.1371/journal.pone.0078770.g010

motion parameter, thermophoresis parameter, magnetic Reynold number and Hartman number

$$\lambda_1=\frac{\epsilon_1 c}{\mu d_1},\ x=\frac{\bar{x}}{\lambda},\ y=\frac{\bar{y}}{d_1},\ t=\frac{c\bar{t}}{\lambda},\ p_m=p+\frac{1}{2}Re\delta\frac{\mu_e(H^+)^2}{\rho c^2},$$

$$d=\frac{d_2}{d_1},$$

$$\gamma=\frac{\bar{T}-T_0}{T_1-T_0},\ u=\frac{\bar{u}}{c},\ \delta=\frac{d_1}{\lambda},\ \bar{S}_{ij}=\frac{d_1\bar{S}_{ij}}{\mu c}\ (\text{for}\ i,j=1,2,3),\ v=\frac{\bar{v}}{c},$$

$$Gc=\frac{g\alpha d_1^3(C_1-C_0)}{\nu^2},\ Gt=\frac{g\alpha d_1^3(T_1-T_0)}{\nu^2},\quad S=\frac{H_0}{c}\sqrt{\frac{\mu_e}{\rho}},$$

$$E=\frac{-\bar{E}}{cH_0\mu_e},$$

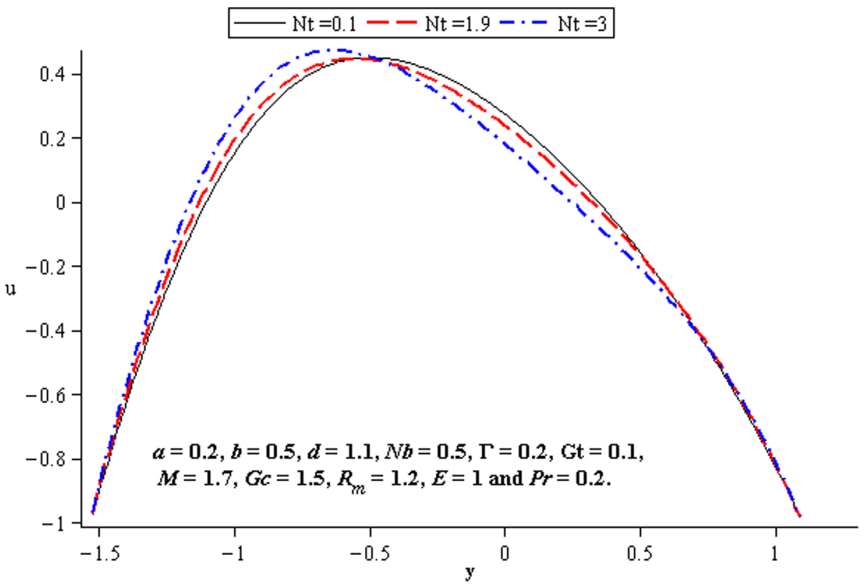

Figure 11. Influence of Nt on u.
doi:10.1371/journal.pone.0078770.g011

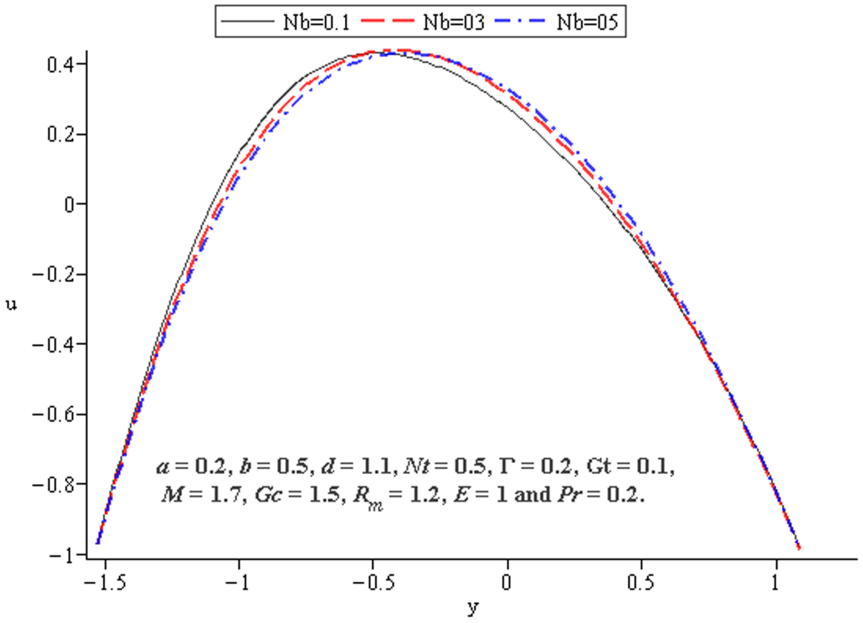

Figure 12. Influence of Nb on u.
doi:10.1371/journal.pone.0078770.g012

$$Nb=\frac{\tau D_B(C_1-C_0)}{\alpha},\quad R_m=\sigma\mu_e d_1 c,\quad Re=\frac{cd_1\rho}{\mu},\quad b=\frac{\bar{b}_1}{\bar{d}_1},\quad h_2=\frac{\bar{h}_2}{\bar{d}_1},\quad \Omega=\frac{\bar{C}-C_0}{C_1-C_0},\quad a=\frac{\bar{a}_1}{\bar{d}_1},\quad \bar{h}_{\bar{y}}=-\bar{\phi}_{\bar{x}},\quad \mu_1=\frac{\bar{\mu}_1 c}{d_1},$$

$$\phi=\frac{\bar{\phi}}{H_0 d_1},\qquad u=\frac{\partial\Psi}{\partial y},$$

$$v=-\delta\frac{\partial\Psi}{\partial x},\quad \zeta_3=\frac{\beta_3 c^2}{\mu d_1^2},\quad h_1=\frac{\bar{h}_1}{\bar{d}_1},\quad \mathrm{Pr}=\frac{\nu}{\alpha},\quad \zeta_2=\frac{\beta_2 c^2}{\mu d_1^2},\quad \zeta_1=\frac{\beta_1 c^2}{\mu d_1^2}$$

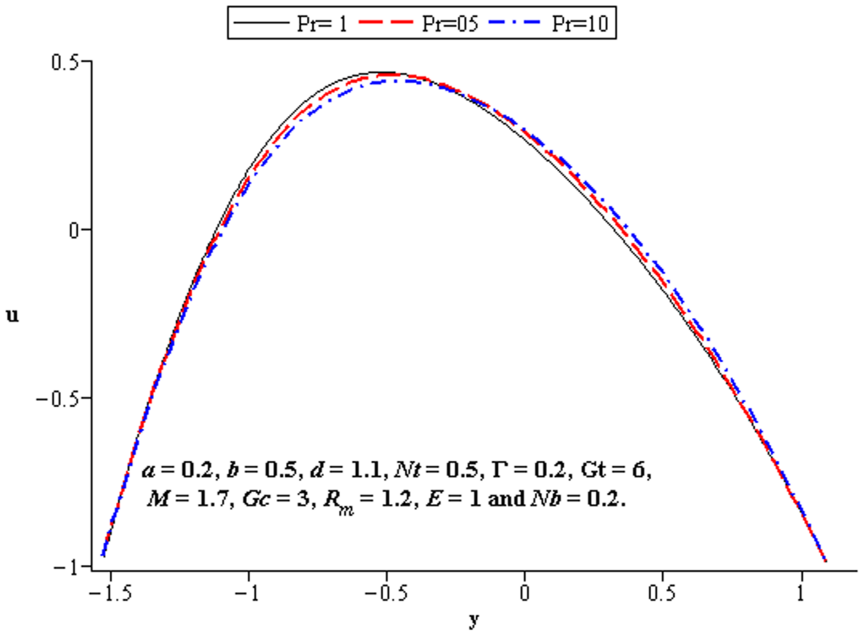

Figure 13. Influence of Pr on u.
doi:10.1371/journal.pone.0078770.g013

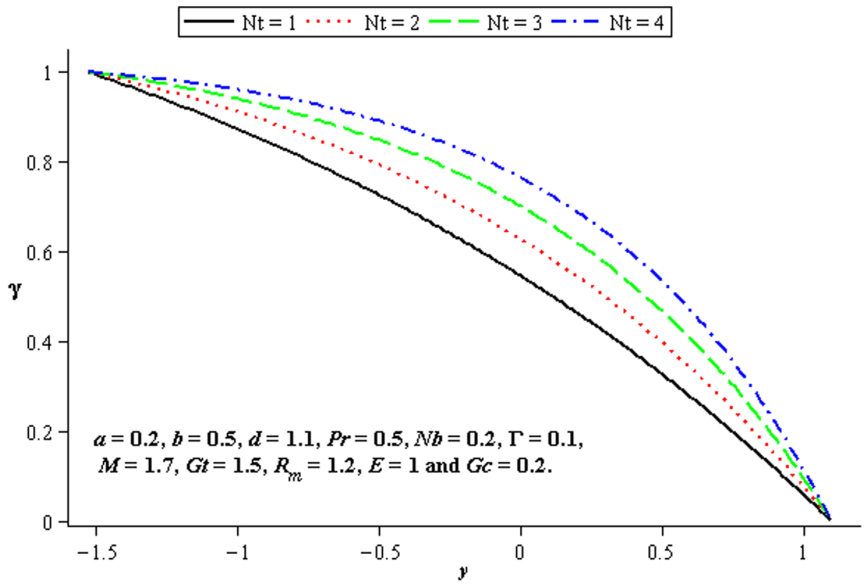

Figure 14. Influence of Nt on γ.
doi:10.1371/journal.pone.0078770.g014

$$Nt=\frac{\tau D_T(T_1-T_0)}{\alpha T_m},\quad b=\frac{a_2}{d_1},\quad \bar{h}_{\bar{x}}=\bar{\phi}_{\bar{y}},\quad M^2=ReS^2R_m,\quad \lambda_2=\frac{\epsilon_2 c}{\mu d_1},\tag{20}$$

and then employing long wavelength and low Reynolds number approximation, the dimensionless forms of above equations in terms of stream function Ψ and magnetic force function ϕ can be expressed as

$$\frac{\partial^4\Psi}{\partial y^4}+2\Gamma\frac{\partial^2}{\partial y^2}\left(\frac{\partial^2\Psi}{\partial y^2}\right)^3-M^2\frac{\partial^2\Psi}{\partial y^2}=-Gt\frac{\partial\gamma}{\partial y}-Gc\frac{\partial\Omega}{\partial y}\tag{21}$$

$$\frac{\partial p}{\partial x}=\frac{\partial^3\Psi}{\partial y^3}+2\Gamma\frac{\partial}{\partial y}\left(\frac{\partial^2\Psi}{\partial y^2}\right)^3-M^2\left(\frac{\partial\Psi}{\partial y}+1\right)+Gt\gamma+Gc\Omega,\tag{22}$$

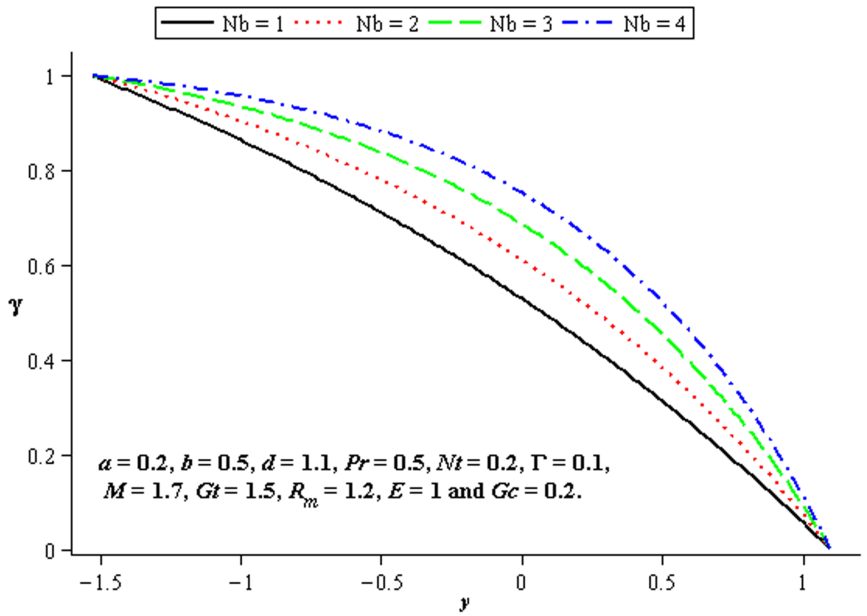

Figure 15. Influence of Nb on γ.
doi:10.1371/journal.pone.0078770.g015

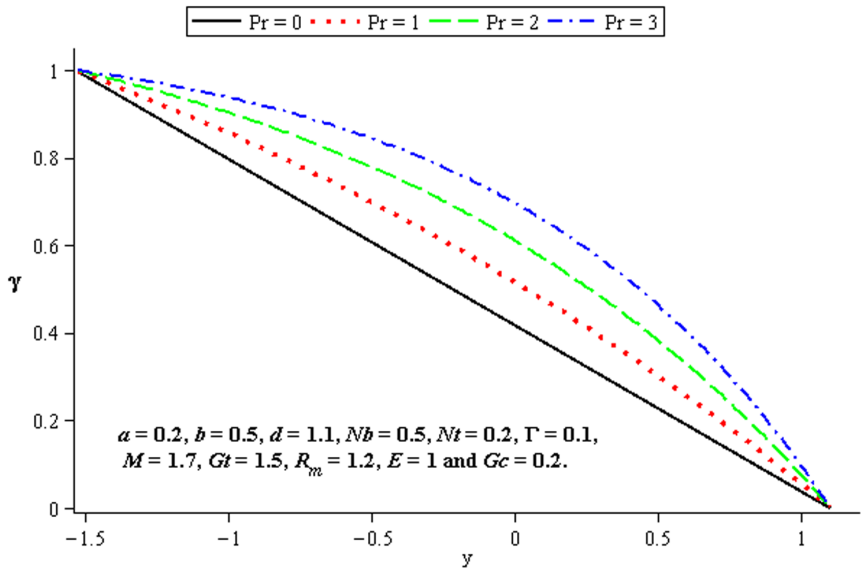

Figure 16. Influence of Pr on γ.
doi:10.1371/journal.pone.0078770.g016

$$\frac{1}{\Pr}\frac{\partial^2\gamma}{\partial y^2}+Nb\frac{\partial\gamma}{\partial y}\frac{\partial\Omega}{\partial y}+Nt\left(\frac{\partial\gamma}{\partial y}\right)^2=0, \tag{23}$$

$$\frac{\partial^2\Omega}{\partial y^2}+\frac{Nt}{Nb}\frac{\partial\gamma}{\partial y}=0, \tag{24}$$

$$\frac{\partial^2\phi}{\partial y^2}=R_m(E-\frac{\partial\Psi}{\partial y}) \tag{25}$$

where $\Gamma=\zeta_1+\zeta_2$.

The dimensionless boundary conditions are given by

$$\begin{aligned}&\Psi=\frac{F}{2},\quad \frac{\partial\Psi}{\partial y}=-1,\ \gamma=0,\ \Omega=0,\phi=0\quad at\\ &y=h_1=1+a\cos(2\pi x),\\ &\Psi=-\frac{F}{2},\quad \frac{\partial\Psi}{\partial y}=-1,\gamma=1,\Omega=1,\phi=0\ \ at\\ &y=h_2=-d-b\cos\left(2\pi x+\phi'\right),\end{aligned} \tag{26}$$

with $a^2+b^2+2ab\cos\phi'\le(1+d)^2$. The dimensionless time mean flow rate F in the wave frame is related to the dimensionless time

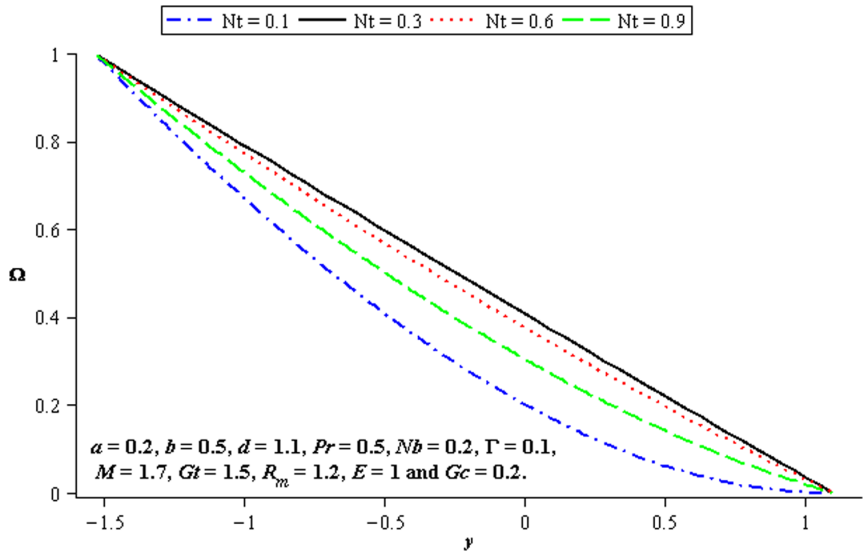

Figure 17. Influence of Nt on Ω.
doi:10.1371/journal.pone.0078770.g017

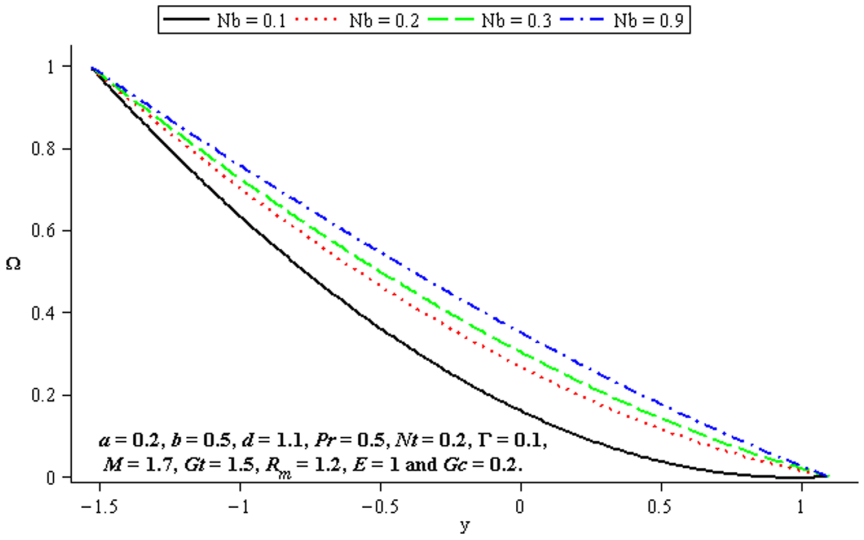

Figure 18. Influence of Nb on Ω.
doi:10.1371/journal.pone.0078770.g018

mean flow rate θ in the laboratory frame by the following expressions

$$\theta = F + 1 + d, \qquad F = \int_{h_2}^{h_1} \frac{\partial \Psi}{\partial y}\, dy. \tag{27}$$

Results and Discussion

Our main interest in this section is to examine the velocity (u), temperature (γ), concentration (Ω), pressure rise per wavelength (ΔP_λ), induced magnetic field (h_x) for the influence of local Grashof number (Gt), Deborah number (Γ), mass Grashof number (Gc), Prandtl number (Pr), Brownian motion parameter (Nb), Hartman number (M), magnetic Reynolds number (R_m) and thermophoresis parameter (Nt).

4.1. Pumping characteristics

This subsection illustrates the behavior of emerging parameters Nt, Nb, Γ,Gt, Gc, and M on pressure rise per wavelength ΔP_λ. The dimensionless pressure rise per wavelength versus time-averaged flux θ has been plotted in the Figs. 1–6. Here the upper right-hand quadrant (I) denotes the region of peristalsis pumping, where $\theta > 0$ (positive pumping) and $\Delta P_\lambda > 0$ (adverse pressure gradient). Quadrant (II), where $\Delta P_\lambda < 0$ (favorable pressure gradient) and $\theta > 0$ (positive pumping), is designated as augmented flow (copumping region). Quadrant (IV), such that $\Delta P_\lambda > 0$ (adverse pressure gradient) and $\theta < 0$, is called retrograde or backward pumping. The flow is opposite to the direction of the

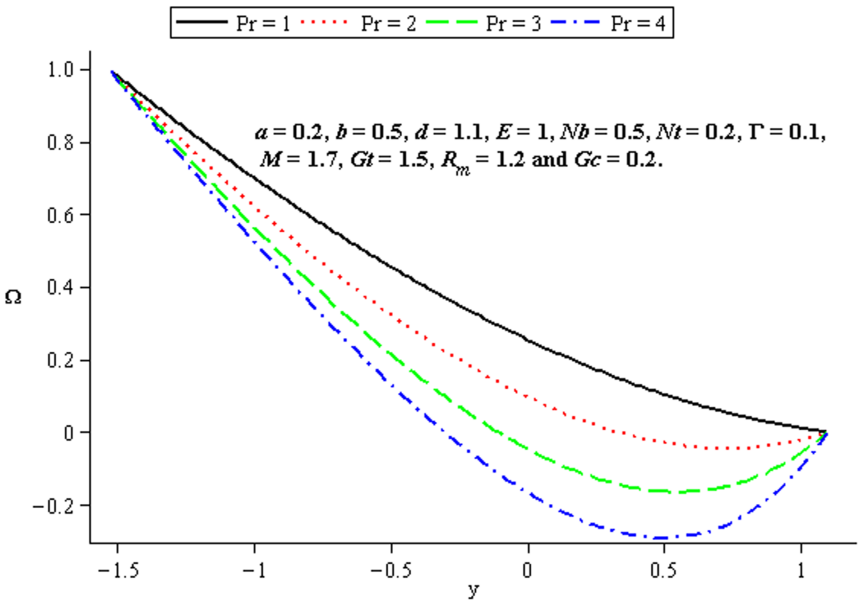

Figure 19. Influence of Pr on Ω.
doi:10.1371/journal.pone.0078770.g019

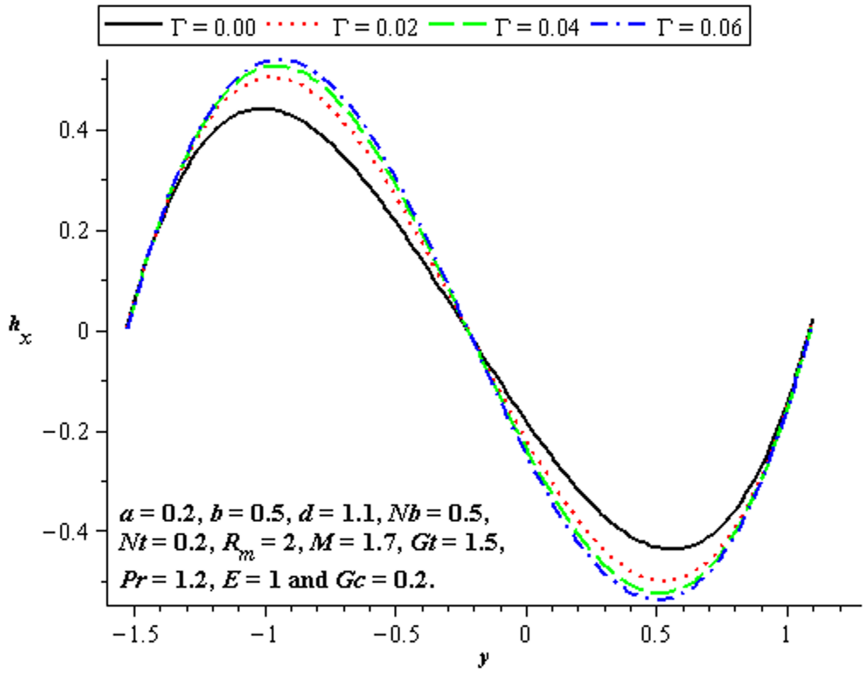

Figure 20. Influence of Γ on h_x.
doi:10.1371/journal.pone.0078770.g020

peristaltic motion and there is no flow in the last (Quadrant (*III*)). There is an inverse linear relation between ΔP_λ and θ. It is noticed from Figs. 1–2 and 4–5 that Δp_λ increases with *Nt*, *Nb*,*Gt* and *Gc* in all the pumping regions. Fig. 3 shows that pumping rate increases by increasing Γ in pumping region. There are specific values of θ for which there is no difference between viscous and third order nanofluids. On the other hand, in the copumping region the pumping rate decreases with the increase in Deborah number. Fig. 6 shows that Δp_λ decreases with *M* in copumping region.

4.2 Flow characteristics

The variations of Γ, *Gc*, *Gt*,θ, *Nt*, *Nb*, and Pr on the velocity have been plotted in this subsection. Fig. 7 shows that there is an increase in velocity at the centre of the channel when Γ increases. We see a little influence of Deborah number on velocity near the

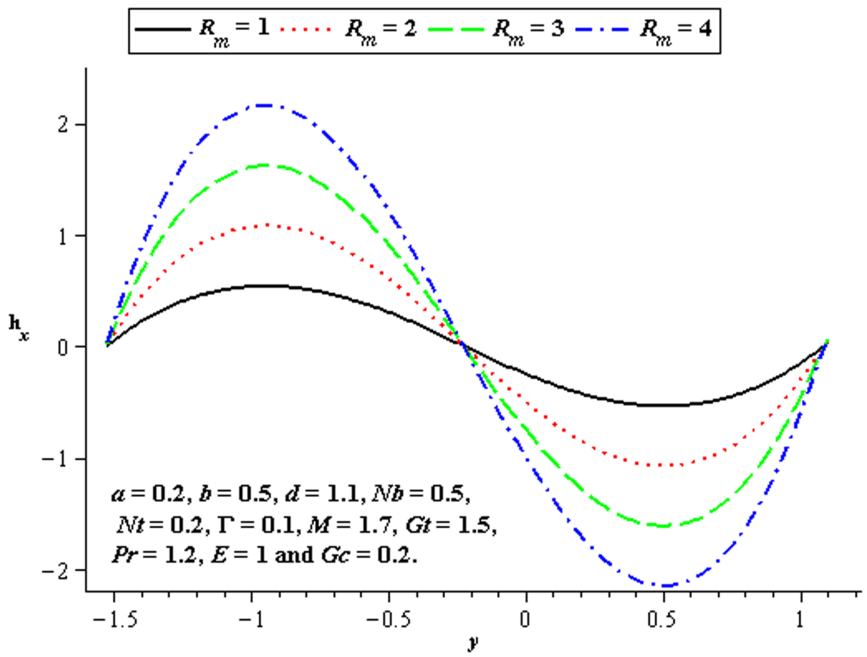

Figure 21. Influence of R_m on h_x.
doi:10.1371/journal.pone.0078770.g021

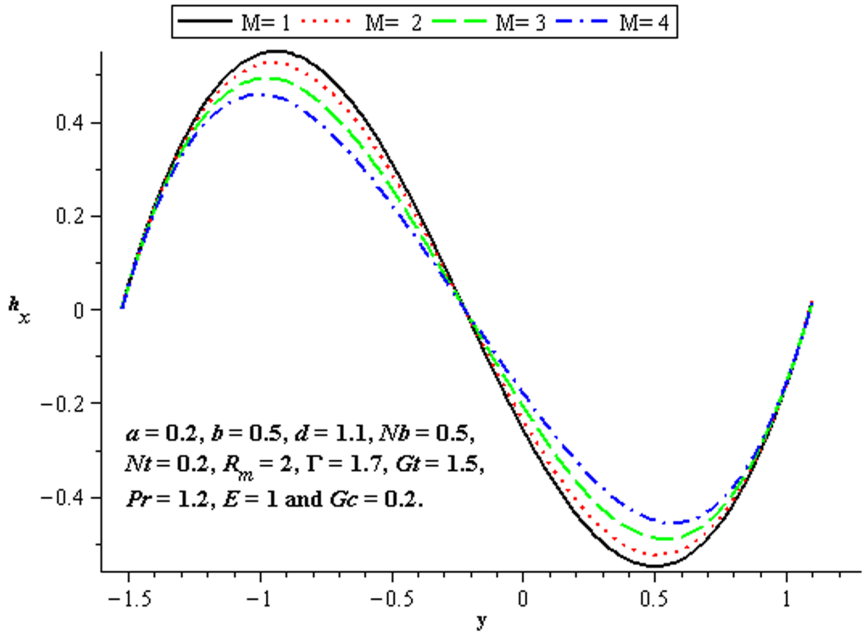

Figure 22. Influence of M on h_x.
doi:10.1371/journal.pone.0078770.g022

walls of channel. However, magnitude of the velocity of third order nanofluid is more than viscous nanofluid. Figs. 8 and 9 depict the influence of local and mass Grashof number. Clearly the velocity increases near the lower wall. Increase in θ supports the motion in the channel which is shown in Fig. 10. Fig. 11 shows the influence of Nt on velocity distribution. Interestingly an increasing thermophoresis leads to an increase in the fluid velocity at the lower wall of channel. There is a considerable variation near the walls $y = h_1$ and $y = h_2$ for Nb and Pr (Figs. 12–13).

4.3 Heat transfer characteristics

Effect of heat transfer on peristalsis is shown in the Figs. 14–16. Figs. 14 and 15 depict the effects of Brownian motion parameter (Nb) and thermophoresis parameter (Nt) on the temperature profile. One can observe that the temperature profile is an increasing function of Nb and Nt between the walls $y = h_1$ and $y = h_2$. In Fig. 16, we observed the effects of Pr on the temperature profile γ by fixing the other parameters. This Fig. indicates that the temperature increases with the increase of Pr.

4.4 Mass transfer characteristics

Influence of mass transfer on peristalsis is shown in the Figs. 17–19. Figs. 17 and 18 depict that the concentration distribution increases at the upper and lower walls of channel when Nt and Nb are increased. Fig. 19 shows the effect of Pr on the concentration when the other parameters are fixed. It shows increasing behavior of Pr on concentration distribution Ω near the walls h_1 and h_2.

4.5 Induced magnetic field characteristics

The variations of Γ, R_m and M on the induced magnetic field have been plotted in the Figs. 20–22. Fig. 20 shows that there is an increase in h_x when Γ increases. We see that magnitude of the induced magnetic field in third order nanofluid is more than

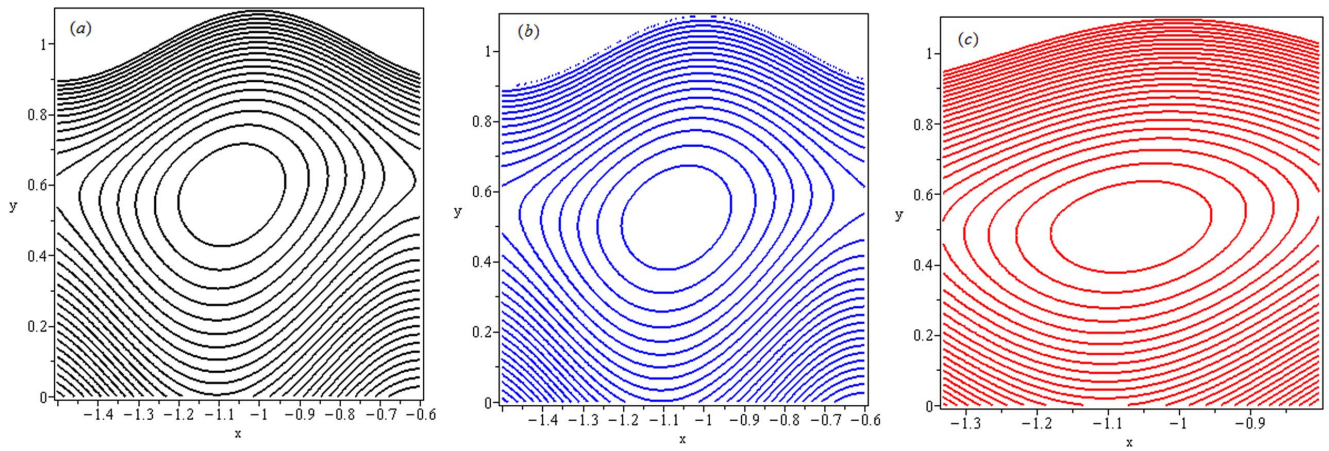

Figure 23. Streamlines for Gt (a): 0.0, (b): 0.1 and (c): 0.2.
doi:10.1371/journal.pone.0078770.g023

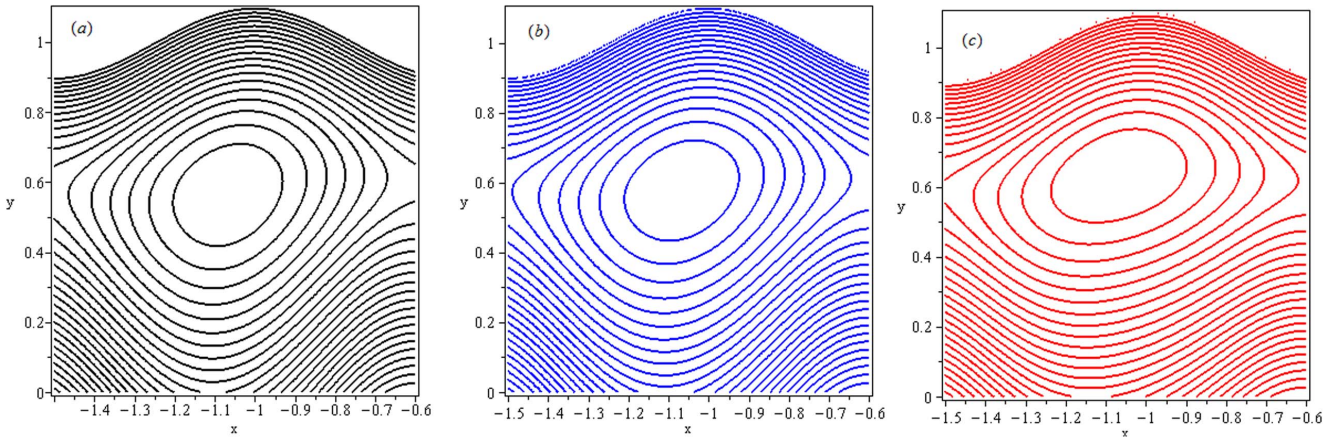

Figure 24. Streamlines for *Nt* (a): 0, (b): 5 and (c): 11.
doi:10.1371/journal.pone.0078770.g024

viscous nanofluid. Figs. 21 and 22 depict the influence of R_m and M. Clearly the h_x increases near the lower half of channel.

4.6 Trapping

Trapping phenomenon is shown in the Figs. 23 and 24 for different values of Gt and Nt respectively. Trapping is an interesting aspect of peristaltic motion. It is the formation of a bolus of fluid by the closed streamlines. Fig. 23 is made for increasing values of Gt. We note that trapping exists for $Gt = 0, 0.1, 0.2$ in the upper part of channel. It is observed that number of closed streamlines circulating the bolus reduce in number as we increase the values of local Grashof number. Meanwhile size of trapped bolus increases. Streamlines are plotted in Fig. 24 to see the effects of thermophoresis parameter (Nt). Clearly, the size of trapped bolus increases when Nt increases from 0 to 11. An upper shift and flatness of bolus along with reduced closed streamlines is observed.

Conclusions

A detailed analysis is presented for peristaltic transport of third order nanofluid in an asymmetric channel with an induced magnetic field and mixed convection. The main findings of the presented study are listed below.

- Pumping rate increases with Gt, Nb and Gc while it decreases with Nt in all pumping regions.
- Velocity distribution is increasing functions of Deborah number at the centre of channel. Absolute value of axial velocity and pressure rise in third order nanofluid is larger than viscous nanofluid.
- Influence of Nb and Nt on mass distribution is opposite to temperature distribution.
- Temperature distribution is an increasing function of Brownian motion parameter (Nb) and thermophoresis parameter (Nt).
- Induced magnetic field increases with R_m and it decreases with M.

Author Contributions

Conceived and designed the experiments: SN. Performed the experiments: SN. Analyzed the data: SN. Contributed reagents/materials/analysis tools: SN. Wrote the paper: SN. Design of problem: SN. Mathematical formulation: SN.

References

1. Latham TW (1966) Fluid motion in a peristaltic pump. MIT Cambridge MA, 1966.
2. Shapiro AH, Jaffrin MY, Weinberg SL (1969) Peristaltic pumping with long wavelengths at low Reynolds number J. Fluid Mech 37: 799–825.
3. Tripathi D, Pandey SK, Das S (2010) Peristaltic flow of viscoelastic fluid with fractional Maxwell model through a channel. Appl Math Comput 215: 3645–3654.
4. Tripathi D, Pandey SK, Das S (2011) Peristaltic transport of a generalized Burgers' fluid: Application to the movement of chyme in small intestine. Acta Astronautica 69: 30–39.
5. Abd Elmaboud Y, Mekheimer KhS (2011) Non-linear peristaltic transport of a second-order fluid through a porous medium. Applied Mathematical Modelling 35: 2695–2710.
6. Hayat T, Mehmood OU (2011) Slip effects on MHD flow of third order fluid in a planar channel. Comm nonlinear Sci Num Simulation 16: 1363–1377.
7. Hayat T, Noreen S, Alsaedi A (2012) Slip and induced magnetic field effects on the peristaltic transport of a Johnson-Segalman fluid. App Math Mech 33:1035–1048.
8. Mekheimer KhS, Abd Elmaboud Y (2008) Peristaltic flow of a couple stress fluid in an annulus: application of an endoscope. Phys Lett A 387: 2403–2415.
9. De Vries K, Lyons EA, Bavard J, Levi CS, Lindsay DJ (1990) Contractions of inner third of the myometrium. Am J Obslet Gynecol 162: 679–682.
10. Das K (2012) Effects of Slip and Heat Transfer on MHD Peristaltic Flow in An Inclined Asymmetric Channel. Iranian J Math Sci Informatics 7: 35–52.
11. Kothandapani M, Srinivas S (2008) Peristaltic transport of a Jeffrey fluid under the effect of magnetic field in an asymmetric channel, Int J Non-LinearMech 43: 915–924.
12. Akbar NS, Nadeem S, Hayat T, Obaidat S (2012) Peristaltic flow of a Williamson fluid in an inclined asymmetric channel with partial slip and heat transfer. Int J of Heat and Mass Transfer 55: 1855.1862.
13. Noreen S, Hayat T, Alsaedi A, Qasim M (2013) Mixed convection, heat and mass transfer in peristaltic flow with chemical reaction and inclined magnetic field, Int J Phy 87: 889–896.
14. Srinivas S, Gayathri R, Kothandapani M (2011) Mixed convection heat and mass transfer in peristaltic flow an asymmetric channel with peristalsis. Commun Nonlin Sci Num Simul 16:1845–1862.
15. Srinivas S, Kothandapani M (2008) Peristaltic transport in an asymmetric channel with heat transfer- A note, Int Comm Heat Mass Transfer 35: 514–522.
16. Choi SUS (1995) The Proceedings of the ASME. Int Mech Eng Congress and Exposition, San Francisco, USA, ASME, FED 231/MD 66:99–105.
17. Nield DA, Kuznetsov AV (2009) The Cheng-Minkowycz problem for natural convective boundary-layer flow in a porous medium saturated by a nanofluid. Int J Heat and Mass Transf 52: 5792.5795.

18. Nield DA, Kuznetsov AV (2011) The Cheng-Minkowycz problem for the double-diffusive natural convective in a porous medium saturated by a nanofluid, Int J Heat Mass Transfer 54:374–378.
19. Motsumi TG, Makinde OD (2012) Effects of thermal radiation and viscous dissipation on boundary layer flow of nano fluids over a permeable moving flat plate, Phys Scr 86:045003–0450010.
20. Mehmoodi M (2011) Numerical simulation of free convection of nano fluid in a square cavity within inside heater, Int J Thermal Sci 50: 2161–2175.
21. Makinde OD, Aziz A (2011) Boundary layer flow of a nano fluid past a stretching sheet with a convective boundary condition, Int J Thermal Sci 50: 1326–1332.
22. Arife AS, Vanani SK, Soleymani F (2013) The Laplace Homotopy Analysis Method for solving a general fractional diffusion eqution arising in nano-hydrodynamics, J Comput Theor NanoSci 10: 33–36.
23. Asproulis N, Drikakis D (2010) Surface roughness effectin micro and nanaofluidic devices, J Comput Theor NanoSci 7: 1825–1830.
24. Gavili A, Ebrahimi S. Sabbaghzadeh J (2011) The enhancement of heat in a two- dimensional enclosure utilized with nanofluids containing cylindrical nanoparticles, J Comput Theor NanoSci 8: 2362–2375.
25. Jancar J, Jancarova E, Zidek J (2010) Combining reputation dynamics and percolation inmodeling viscoelastic response of collagen based nanoparticles, J Comput Theor NanoSci 7: 12557–1264.
26. Nusrati R, Hadigol M, Raisee M, Nourbakhsh A (2012) Numerical investigationon laminar flow due to suddenexpansion usind nanofluids, J Comput theo NanoSci 9:2217–2217.
27. Ozsoy O, Harigaya K (2011) Theoratical calculation of shrinking and stretching in bond structure of monolayer graphite flake via hole doping treatment, J Comput Theor NanoSci 8:31–37.
28. Ono T, Fujimoto Y, Tsukamoto S (2012) First-Principles calculation method for obtaining scattering waves to investigate transport properties of nanostructures, Quantum Matter 1 4–19.
29. Bose PK, Paitya N, Bhattachary S, De D, Saha S, et al. (2012) Influence of light waves on the effective electron mass in quantum wells, wires, inversion layers and superlattices, Quantum Matter 1:89–126.
30. Tüzün B, Erkoç S (2012) Structural and electronic properties of unusual carbon Nanorods, Quantum Matter 1: 136–148.
31. Narayanan M, Peter AJ (2012) Pressure and temperature induced non-linear optical properties in a narrow band gap quantum dot, Quantum Matter 1: 53–58.
32. Paitya N, Bhattacharya S, De D, Ghatak KP (2012) Influence of quantizing magnetic field on the Fowler-Nordheim field emission from non-parabolic materials, Quantum Matters 1:63–85.
33. Akbar NS, Nadeem S (2011) Endoscopic effects on peristaltic flow of a nanofluid, Commun Theor Phys 56: 761–768.
34. Akbar NS, Nadeem S, Hayat T, Hendi AA (2012) Peristaltic flow of a nanofluid with slip effects, Meccanica 47:1283–1294.